New Hybrid Perovskites/polymer composites for the photodegradation of organic dyes

Chaima Brahmi, Mahmoud Benltifa, Cyril Vaulot, Laure Michelin, Frédéric Dumur, Aissam Airoudj, Fabrice Morlet-Savary, Bernard Raveau, Latifa Bousselmi, Jacques Lalevée

New Hybrid Perovskites/polymer composites for the photodegradation of organic dyes

Chaima Brahmi[a,b,c,d], Mahmoud Benltifa*[c], Cyril Vaulot[a,b], Laure Michelin[a,b], Frédéric Dumur [e], Aissam Airoudj[a,b], Fabrice Morlet-Savary[a,b], Bernard Raveau[f], Latifa Bousselmi[c], Jacques Lalevée* [a,b]

[a] University of Haute-Alsace, CNRS, IS2M UMR 7361, F-68100 Mulhouse, France

[b] University de Strasbourg, France

[c] Laboratory of Wastewaters and Environment, Center for Water Research and Technologies CERTE, BP 273, Soliman 8020, Tunisia

[d] University of Carthage, National Institute of Applied Sciences and Technology, Tunis 1080, Tunisia

[e] Aix Marseille Univ, CNRS, ICR, UMR7273, F-13397 Marseille (France)

[f] Laboratoire CRISMAT, UMR 6508 Normandie Université, CNRS, ENSICAEN, UNICAEN, Caen, France

*Corresponding authors: mahmoud.benltifa@certe.rnrt.tn; Jacques.lalevee@uha.fr

Abstract

Recently, many researchers have focused their attentions on associating perovskites with polymers in order to enhance their processability and rigidity while protecting their interesting environmental properties. Therefore, this work reports the successful development of two different perovskites/polymer composites via a simple, rapid, low-cost and eco-friendly photopolymerization process under mild visible Light Emitting Diode LED@405nm irradiation. The as-synthesized composites exhibit excellent photocatalytic activity towards the removal of the Acid Black dye from water, reaching approximatively 95% under just 30 min of UV light irradiation. The fruitful hybridization between the perovskite and the acrylate monomer allowed the collect and reuse of this photocatalyst for several successive cycles without external usual time-consuming methods. Furthermore, the new as-fabricated shaped materials were fully characterized by numerous characterization techniques including SEM, TEM, EDX, DRX, AFM, DMA and ATG which have verified on one side the successful immobilization of the perovskites into the polymer and the structural

stability of the photocatalysts after hybridization and in the other side the high rigidity and thermal stability of the obtained molded composites.

1. Introduction

Semiconductors heterogenous photocatalysis has recently attracted many researcher's interests thanks to its various green and sustainable environmental applications including wastewater treatment via the elimination of recalcitrant organic pollutants form water[1], hydrogen production[2], decrease of the CO_2 emission in the atmosphere by its transformation to fuels[3] as well as the purification of air by removing NO_x and SO_X pollutants[4]. Moreover, the photocatalytic processes are generally carried out at ambient temperature with the possible use of the renewable solar irradiation as the source of irradiation while ensuring the total mineralization of the different target pollutants without producing secondary harmful pollution[5]. This degradation method is based on the irradiation of a powder or shaped solid photocatalysts, dispersed in aqueous solution containing pollutants. Once this material absorbs energy equal or higher than its bandgap energy, it produces highly reactive chemicals such as hydroxide and superoxide anions radicals which degrade in their turn the organic compounds[6,7].

The diversified environmental eco-friendly applications of heterogenous photocatalysis have induced the emergence of various materials suitable for such objectives. The most commonly one during the last few decades was titanium dioxide owing to its non-toxicity, low cost, facile synthesis and high chemical stability[8]. However, because of its high bandgap energy (3.0-3.2 e.V), this photocatalyst could only absorb UV light corresponding to just 4% of the solar spectrum emission[9]. Another inconvenient of this material is the fast recombination of the photogenerated electrons-holes pairs[10]. Hence, to overcome these limits, many efforts have been devoted to enhance the TiO_2 photocatalytic performance by decreasing the hole-electron recombination rate via its association with other semiconductors[11] or its doping with metals[8,12] or nonmetal[13] in order to ameliorate its visible light absorbance. In this context, many new catalysts including ZnO[14], WO_3[15], CdS[16], ZnS[17], Polyoxometalates[18],Metals Organics Frameworks[19] were explored.

Among all the various reported photocatalysts, perovskites belong also to an interesting and promising class of materials, fitting with the photocatalytic processes'

features, owing to their chemical and photostability, their low synthesis cost, their modifiable energy bandgap, their high absorption properties, as well as their long charge carrier lifetime and diffusion length[20]. Perovskites were raised from calcium titanium dioxide ($CaTiO_3$) and have generally a cubic crystal structure described by an ABX_3 system, A being a cation larger in size than the cation B that could be either an organic compound such as methyl ammonium (MA^+: $CH_3NH_3^+$) or an inorganic compound such as metals, alkalis (Na, K), lanthanides or rare earth metals (La, Sm, Pr). B in its turn corresponds to a transition metal ion (Sn, Pb, Ge) and X is often an oxygen anion[21,22,23]. Thanks to the countless possible combinations between cations A and B, properties of the resulting materials can be modified to perfectly fit to the future desired applications, such as X-ray imaging[24], solar cells[25], light-emitting diode (LED) devices[26] and photocatalytic applications[21,23]. As examples of suitable perovskites for pollutants photodegradation goals, a methylammonium lead iodide perovskite was applied as visible light semiconductor for the degradation of rhodamine B and methylene blue dyes[5]. Moreover, 4-chlorophenol, rhodamine B and brilliant green were respectively decomposed by a $LaFeO_3$ and $CaTiO_3$ perovskites under visible and UV light irradiation source[27,28].

Despite their beneficial and promising green environmental photocatalytic applications, the use of perovskites as photocatalysts is generally associated with separation, regeneration and recycling difficulties, since they are usually used in their powder forms. Current works are trying to find solutions to this problem by developing new synthetic methods to prepare perovskites thin films and composites materials[21]. Indeed, Eskandari et al. have developed a magnetic $CoFe_2O_4$–$SrTiO_3$ perovskite nanocomposite, applied for the degradation of toxic dyes and easy to collect and reuse thanks to the external magnetic field[22]. Raja et al. have also immobilized a perovskite ($CsPbBr_3$) into a hydrophobic macroscale polymer matrix which enhanced the water and light stability of the initial photocatalysts[29].

In this context, this article reports on the development of a new perovskite/polymer composite exhibiting an excellent efficiency towards the removal of organic pollutants from water even without the addition of oxidizing agents. The immobilization of the chosen perovskites was carried out by a photopolymerization process which is an eco-friendly synthetic method using a harmless and low-cost LED irradiation source avoiding the release of volatile organic compounds[30]. The obtained shaped materials display a good robustness, processability and stability of the polymers and the high photocatalytic properties of the

perovskites. Therefore, this approach is a suitable and cost-effective solution to collect and reuse these photocatalysts avoiding then the time-consuming usual methods of separation and regeneration including filtration and centrifugation.

Perovskites used in this work were $Nd_{0.9}TiO_3$ and $LaTiO_3$. These perovkistes were chosen based on a bibliographic study. In fact, titanate perovskites are thermically stable and are characterized by a remarkable high corrosion resistance which is suitable to their photocatalytic applications[31]. Moreover, lanthanum perovskites constituted by lanthanum at A site and transition element at site B, were involved in their powdered forms, previously in many catalytic reactions such as the degradation of methylene blue, neutral red, rhodamine B and congo red[32] and atrazine[33]. To support the choice of Acid Black as a model pollutant for the monitoring of the photocatalytic ability of the different developed composites, it has to be noticed that this dye can be found in textile industries effluents and to its attested harmful carcinogenic effects totally support the ongoing efforts to develop efficient methods to mineralize this dye [34,35].

To confirm the successful hybridization between the perovskites and the polymers, the obtained composites were fully characterized by several techniques including Thermogravimetric Analysis (TGA), Scanning Electron Microscopy (SEM), Transmission Electron Microscopy (TEM), Energy-dispersive X-ray analyses (EDX), X- Ray Diffraction analysis (XRD), BET specific surface area, Atomic Force Microscopy (AFM), Dynamic Mechanical Analysis (DMA) and UV-Visible diffuse reflectance spectroscopy. Furthermore, the photocatalytic performances of these photocatalysts were tested for 10 successive degradation cycles of Acid Black and the degradation mechanism was identified thanks to the monitoring of the dye decomposition kinetics in the presence of different scavengers and under different atmospheres.

2. Experimental section

2.1. Chemical compounds

The compounds used for the composite's synthesis are the TMPTA (from Allnex), *Bis*(4-*tert*-butylphenyl)iodonium hexafluorophosphate (Iod or Speedcure 938) and phenyl *bis*(2,4,6-

trimethylbenzoyl)phosphine oxide (BAPO or Speedcure BPO) were obtained from Lambson Ltd (UK). For the scavenging experiments, EDTA (Ethylenediaminetetraacetic acid) and 2,2,6,6-tetramethyl-1-piperidinyloxy (TEMPO) were purchased from Sigma Aldrich. 4-Methoxyphenol (MEHQ) and titanium dioxide (predominantly rutile and anatase) were acquired from Alfa Aesar. Acid Black dye chosen as a target pollutant to degrade was bought form Sigma Aldrich. Structures of the chemicals used in this work are presented in our previous works[36] (article MOF comme reference).

2.2. Photopolymerization experiments

Photopolymerization experiments were carried out under air by placing the initial resin containing TMPTA as the monomer and iodonium salt and BAPO as the photoinitiating system, in a mold (thickness = 1.3 mm), The resin was subsequently irradiated by a light Emitting Diode LED@405 nm (I_0 = 100 mW/cm^2) and the polymerizations rates were determined by monitoring of the TMPTA double bond located at 4730 cm^{-1} for thick samples using a real-time Fourier transform infrared spectroscopy.

2.3. Photocatalytic activity

Acid Black dye was chosen in this work to investigate the photocatalytic performances of the perovskite/polymer composites under an Omnicure Dynamic lamp, series 1000 lumen (I_0 = 250 mW/cm^2, λ = 320-520 nm). The initial concentration of the target pollutant was fixed to 15 mg/L (24.25 µmol/L) and the volume of the aqueous solution to degrade was equal to 4 mL which corresponds to the volume of the UV analysis cuvette, where the photodegradation experiments were carried out in the presence of the photocomposites pellets.

Dye concentrations were calculated based on its absorbance located at 618 nm, which was monitored with a JASCO V730 spectrophotometer according to the following equation:

Dye degradation (%) = $\left(1 - \frac{Abs\ t}{Abs\ t=0}\right)$ ×100 (eq.1)

Where $Abs\ t = 0$ and $Abs\ t$ are the measured Acid Black absorbances before and after a given time (t) of irradiation.

2.4. Composite's stability

Water stability of the perovskites/polymer composites was investigated by carrying out swelling and dry extract experiments. Moreover, the thermal stability was evaluated by Thermogravimetric Analysis (TGA) technique. Experimental conditions of these tests were detailed in our previous works[36] (reference article MOF).

2.5. Composite's characterization

2.5.1. Morphological and chemical characterizations

A JSM-7900F Scanning Electron Microscopy (SEM) from JEOL with an annular detector from DEBEN for transmission images was used for SEM imaging. Moreover, for chemical characterization, an Energy-dispersive X-ray analysis was carried out via a QUANTAX double detector from Bruker.

2.5.2. Composites structural characterization

A Panalytical X'Pert PRO diffractometer equipped with a Cu X-ray tube (Cu_{Ka} = 0.1542 nm) and and a PIXCel detector was used for XRD experiments. Operating conditions were fixed at 45 kV and 40 mA.

2.5.3. Composites surface topography and rigidity

Roughness and elastic modulus of the developed perovskites/polymer composites were evaluated by Atomic Force Microscopy (AFM) characterization technique with a Bruker Multimode IV, with a Nanoscope V controller and an E "vertical" scanner (Bruker). Moreover, a Peak Force Quantitative Nanomechanical Mapping (PF-QNM, Bruker) method was used for AFM experiments. Details concerning this technique were reported in our previous works[36].

2.5.4. Textural properties and porosity

Porosities of the different developed materials were evaluated from nitrogen adsorption/desorption at 77.35 K with a micromeritics ASAP 2420 instrument. Standard Brunauer, Emmett, and Teller (BET) method were used to calculate the BET specific surface area and the average pore diameter (Gurlich law). The samples were degassed at 25°C for 60 hours on degassing port and weighted. Then, the samples were degassed once again at 25°C for 4 hours on the analysis port to extract the trapped nitrogen. Analyses were realized with

a reactor of the free volume to optimize the measurement and the free volumes were determined after analysis to avoid the pollution of the samples.

2.5.5. Mechanical properties in bulk

Bulk mechanical properties of the synthesized perovskites/polymer composites were characterized by a DMA Mettler Toledo DMA861e.

2.5.6. Optical properties

Reflectance measurements of the polymer as well as the perovskites/polymer composites were evaluated using a UV-visible spectrophotometer (JASCO V-750) equipped with an integrating sphere.

3. Results and discussion

3.1. Synthesis of perovskites/polymer composite by photopolymerization

The different perovskites/polymer composites were prepared by photopolymerization enabling to convert the viscous solution containing the monomer, the photoinitiating system (BPO and IOD), and the perovskites as fillers via a fast LED@405nm illumination avoiding then the possible perovskites degradation caused by the thermal heating which is a necessary step in the classical thermal polymerization. This technique proved to be the most suitable one for the development of such shaped composites thanks to its facile and rapid processability.

Four different monomers were tested during the development of the perovskites/polymer composites, in order to choose the most suitable one, enabling to reach the highest polymerization rates while providing materials stable in water and retaining the excellent photocatalytic activity of the perovskites. The obtained photopolymerization profiles for the free radical polymerization (FRP) are reported in Figure 1.

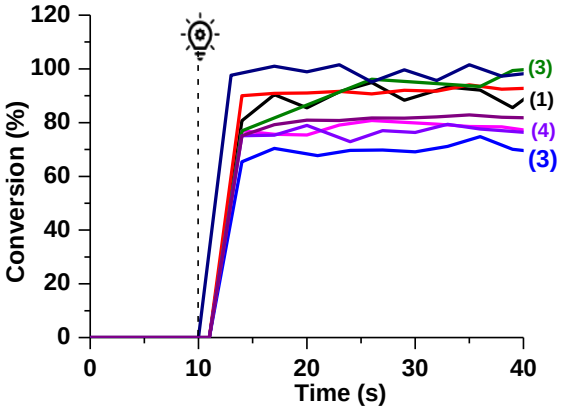

Figure 1. Photopolymerization profiles of acrylate functions (double bond conversion vs irradiation time) under air upon exposure to a LED@405 nm in the presence of BAPO/Iod/ $LaTiO_3$ (0.2%/1%/0.5% (w/w/w)) based on (1) Ebecryl 40, (2) PETIA, (3) SR-610 and (4) TMPTA.

Figure 1 shows that high polymerization rates could be obtained by the different monomers tested for the composites synthesis in the presence of 0.5% of $LaTiO_3$ perovskite. Indeed, the acrylate conversions were respectively of 100%, 88%, 77% and 69% using SR-610 (90 mPa/s), Ebecryl 40 (160 mPa/s), TMPTA (115 mPa/s) and PETIA (1044 mPa/s) as the monomers. Thus, proving that various monomers could be suitable for the obtainment of these composites. However, our previous works on the development of POM/polymer composites showed that the most appropriate monomer for the development of composites with photocatalytic treatment goals is TMPTA owing to its hydrophobic character and average viscosity[37]. This will be verified in the following sections of this article by realizing stability tests in water and photodegradation experiments of the composites synthesized with these different monomers.

The effect of the filler mass percentage present in the initial formulation, on the acrylates functions polymerization rates was studied by varying the amount of the perovskite into the monomer resin (See Figure 2). TMPTA monomer was chosen for these experiments as well as for the full characterization part of this article in order to be able to compare this study with our previous works related to the degradation of organic pollutants by POM/polymer and MOF/polymer composites[18,36].(Articles mof)

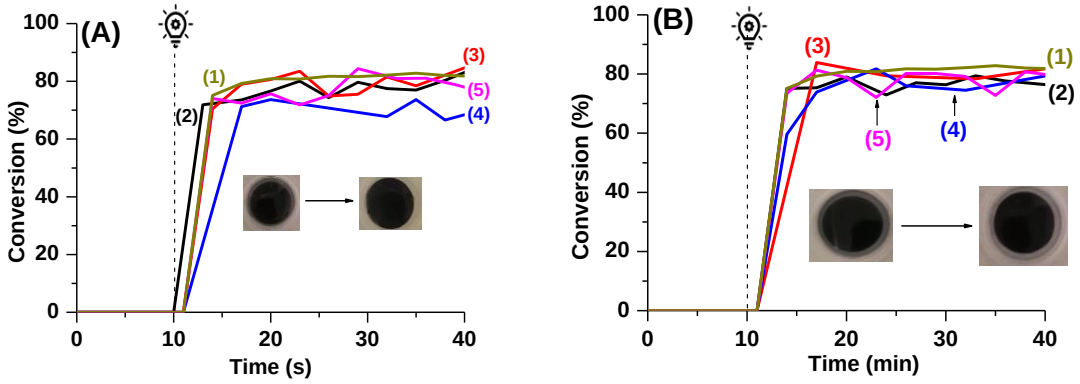

Figure 2. Photopolymerization profiles of acrylate functions (double bond conversion vs irradiation time) under air upon exposure to a LED@405 nm (A) in the presence of BAPO/Iod/$Nd_{0.9}TiO_3$ (1) (0.2%/1%/0% (w/w/w)), (2) (0.2%/1%/0.5% (w/w/w)), (3) (0.2%/1%/1% (w/w/w)), (4) (0.2%/1%/2% (w/w/w)), (5) (0.2%/0%/1% (w/w/w)); (B) in the presence of BAPO/Iod/$LaTiO_3$ (1) (0.2%/1%/0 (w/w/w)), (2) (0.2%/1%/0.5% (w/w/w)), (3) (0.2%/1%/1% (w/w/w)), (4) (0.2%/1%/2% (w/w/w)) and (5) (0.2%/0%/1% (w/w/w)); thickness = 1.3 mm; the irradiation starts at t = 10 s.

Figure 2 (A, B) shows respectively the TMPTA polymerization kinetics under mild irradiation@405nm in the presence of perovskites $Nd_{0.9}TiO_3$ and $LaTiO_3$ with different mass percentages. Remarkably, the final acrylate function conversions (AFCs) weren't almost affected by the addition of the perovskites to the initial TMPTA resin containing BAPO as the photoinitiator and the iodonium salt as the co-initiator, except in the case of the 2% $Nd_{0.9}TiO_3$/polymer composite. Indeed, the AFC reached in 40 seconds decreases from 82% in the absence of the filler to 68.5% in the presence of 2% of $Nd_{0.9}TiO_3$. This could be explained by the inhibition of light penetration by the incorporated catalyst.

In order to compare our current results with our previous works related to the development of new POM/polymer composites where the presence of the iodonium salt as the co-initiator was essential to achieve high photocatalytic performances[18,36], this compound was added to the initial formulations and influence of its presence on the achieved AFCs was examined. Results are shown in Figure 2 (A, B (curves 3 and 5). Indeed, the absence of iodonium salt in the photocurable resin resulted in a slightly decrease of the photopolymerization rates reached after 40 seconds of irradiation, from 84% to 77% and from

81.8% to 79.5% in the case of the 1% $Nd_{0.9}TiO_3$/polymer and the 1% $LaTiO_3$/polymer composites, respectively.

The photocatalytic activity of the different synthesized perovskites/polymer composites will be discussed latter in section 3.4.

3.2. Perovskites/polymer composites stability

Thermal and solvent stabilities are the most important indexes for future industrial environmental applications of the new developed perovskites/polymer composites. Therefore, these two parameters were investigated in this section of the article.

3.2.1. Stability in water

For green and eco-friendly photocatalysis application, water was chosen as the most suitable solvent for the Acid Black photodegradation tests. Therefore, swelling experiments were carried out in this solvent. Dry extract ratio was also calculated to evaluate the monomer loss probability from the composite after contact in water.

Table 1. Acrylates Final Conversion (AFC %), Swelling (%) (in water) and dry extract (%) for the different synthesized perovskites/polymer composites.

	AFC (%)	**Swelling (%)**	**Dry extract (%)**
Polymer based TMPTA	82	10 ± 0.5	100 ± 0.5
0.5% $LaTiO_3$/polymer based TMPTA	77	0 ± 0.5	98 ± 0.5
0.5% $Nd_{0.9}TiO_3$/polymer based TMPTA	83	1.3 ± 0.5	100 ± 0.5
Polymer based Ebecryl 40	92	2 ± 0.5	100 ± 0.5
0.5% $LaTiO_3$/polymer based Ebecryl 40	88	1 ± 0.5	99 ± 0.5
Polymer based PETIA	77	1.8 ± 0.5	100 ± 0.5
0.5% $LaTiO_3$/polymer based PETIA	70	1.2 ± 0.5	98 ± 0.5
Polymer based SR-610	98	56± 0.5	139± 0.5

0.5% $LaTiO_3$/polymer-based SR-610	100	54± 0.5	137± 0.5

The obtained low swelling percentages for the polymer and the composites based TMPTA, Ebecryl 40 and PETIA gathered in Table 1 suggest a highly crosslinked acrylate network even in the presence of the perovskites into the polymers,[38] what is in agreement with the AFCs. However, in the case of the polymer-based SR-610 and the $LaTiO_3$/polymer based SR-610 composite, high obtained swelling rates (56% and 54%) indicate the non-stability of this composite in water which is probably due to the hydrophilic character of the SR-610 monomer, provoking then the leaching of the perovskites into the aqueous solution[37]. Moreover, the high dry extract percentages for the different polymers and their respective composites except those based on SR-610 and presented in Table 1 indicate the low loss probability of the monomer after the photopolymerization process. Therefore, these experiments demonstrate that the TMPTA, PETIA and Ebecryl 40 monomers are ideal candidates for the development of perovskites/polymer composites thanks to their good stability in water in contrast to that observed in SR-610-based polymer.

3.2.2. Thermal stability

Photocatalysts thermal stability is one of the most important parameters to consider for heterogenous photocatalytic industrial activities. Hence, the decomposition temperatures of the different developed materials were investigated. Results are presented in Table 2.

Table 2 : Decomposition temperatures of the polymers, the crystals perovskites and the 0.5% perovskites/polymer composites

Material	**Polymer**	**perovskites/polymer composites**	
		$LaTiO_3$	$Nd_{0.9}TiO_3$
Decomposition temperature(°C)	475	476	478

TGA analyses showed that the different developed composites are characterized by a high thermal stability since they are decomposed at 476°C and 478°C. These temperatures

which are close to that obtained for the polymer free of perovskites (475°C), are thus suitable for the possible photocatalytic application of these materials. Therefore, the immobilization of the perovskites into the polymer matrix didn't affected the thermal stability properties of the polymers.

3.3. Perovskites/polymer composites characterization

Herein, a full characterization of the immobilized perovskites into the polymer based TMPTA, is reported. Thus, investigating the filler presence into the polymer matrix, their structural stability and their dispersion at the surface of the composite, where the photocatalytic reactions occur. Optical and mechanical parameters were also interesting to characterize the possible practical applications.

3.3.1. Morphological and chemical characterization

Morphologies of the synthesized perovskites/polymer composites and the neat polymers based on TMPTA were characterized by Transmission Electron Microscopy (TEM) and Scanning Electron Microscopy (SEM) which showed the dispersion of the perovskite's fillers at the polymer matrix surface. Resulted images are presented in Figure 3.

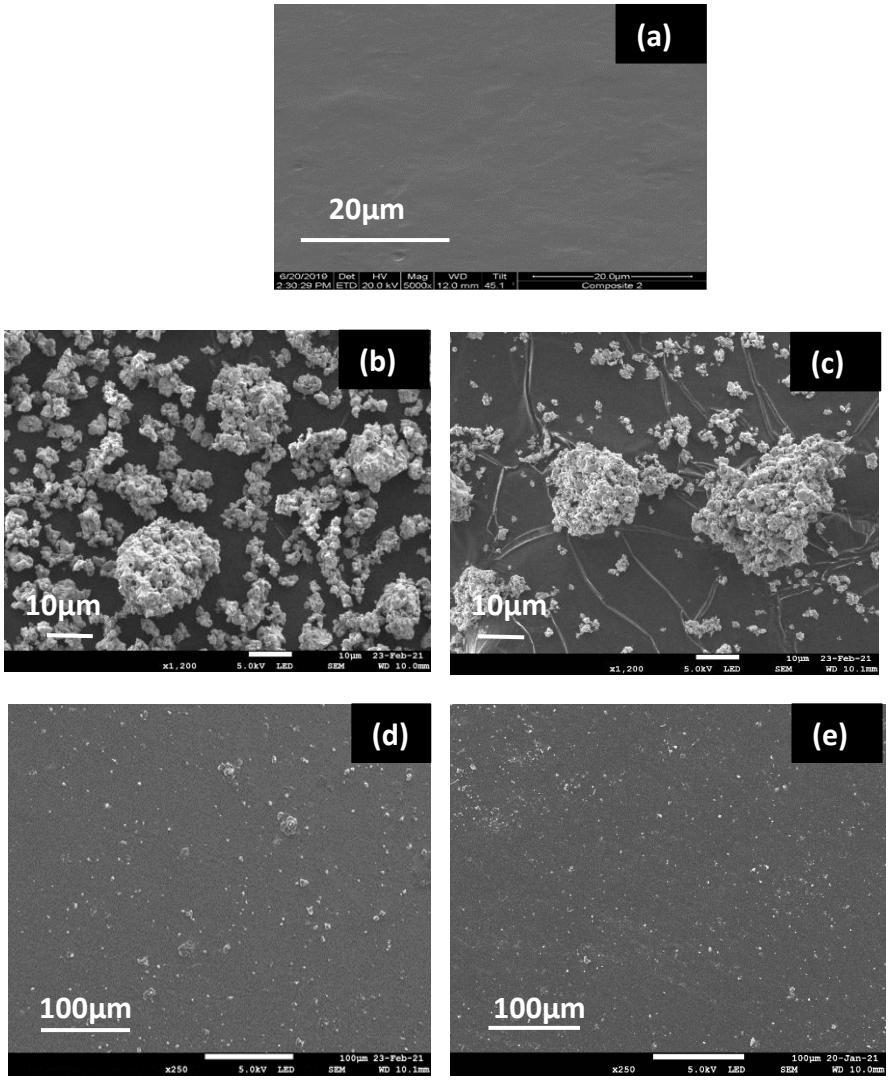

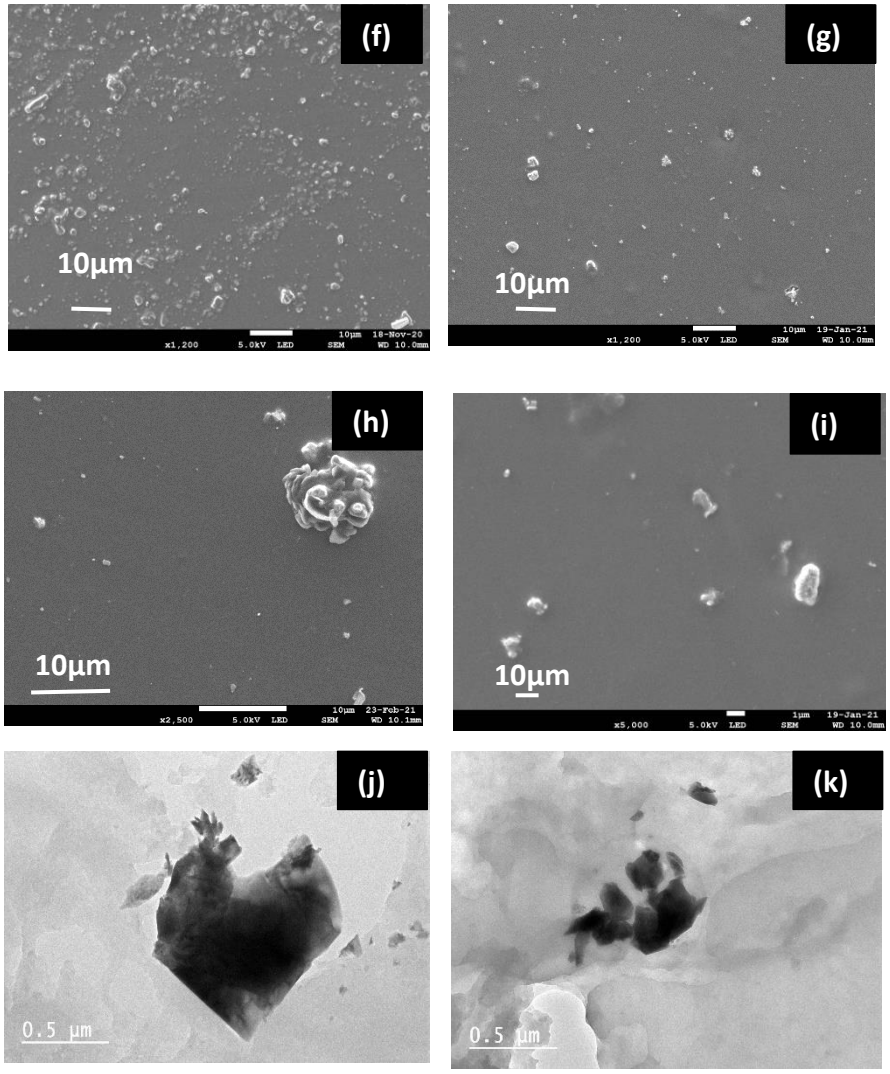

Figure 3. SEM images of (a) Polymer without perovskites, (b) $Nd_{0.9}TiO_3$ powder; (d, f, h) 2% $Nd_{0.9}TiO_3$/polymer composite at different scales; (c) $LaTiO_3$ powder; (e, g, j) 2% $LaTiO_3$/polymer composite at different scales. TEM images of (j) 2% $Nd_{0.9}TiO_3$/polymer composite, (k) 2% $LaTiO_3$/polymer composite.

Based on the Figure 3 (a), the neat polymer based on TMPTA exhibits a homogenous surface. On the opposite, the perovskite-based composites displayed heterogenous surfaces due to the immobilization of the perovskites.

The SEM images of the $Nd_{0.9}TiO_3$ and $LaTiO_3$ powders displayed respectively in Figure 3 (b and c) demonstrate that the morphology of the most perovskites granules are orthorhombic with irregulated agglomerated shape distributions. Such observations were already reported when studying the $LaTiO_3$ perovskite synthesis[39]. Furthermore, the SEM images of the 2% $Nd_{0.9}TiO_3$/polymer and 2% $LaTiO_3$/polymer composites shown respectively in Figure 3 (d, e, f, g, h and i) revealed that these materials exhibited an heterogenous surface containing micrometric perovskites aggregates of different sizes. Also, Figure 3 (j, k) shows TEM images of the two perovskites/polymer composites indicating the presence of these photocatalysts at the polymer surface. Moreover, as represented in Figure S1, a cutaway view of the synthesized materials has proved that the perovskites were present in the surface and the bulk of the composite too.

The perovskites dispersion at the surface of the polymer based TMPTA was further investigated via Energy Dispersive X-ray (EDX) analyses which confirmed also the successful hybridization of the perovskites/polymer composites (See Figure 4).

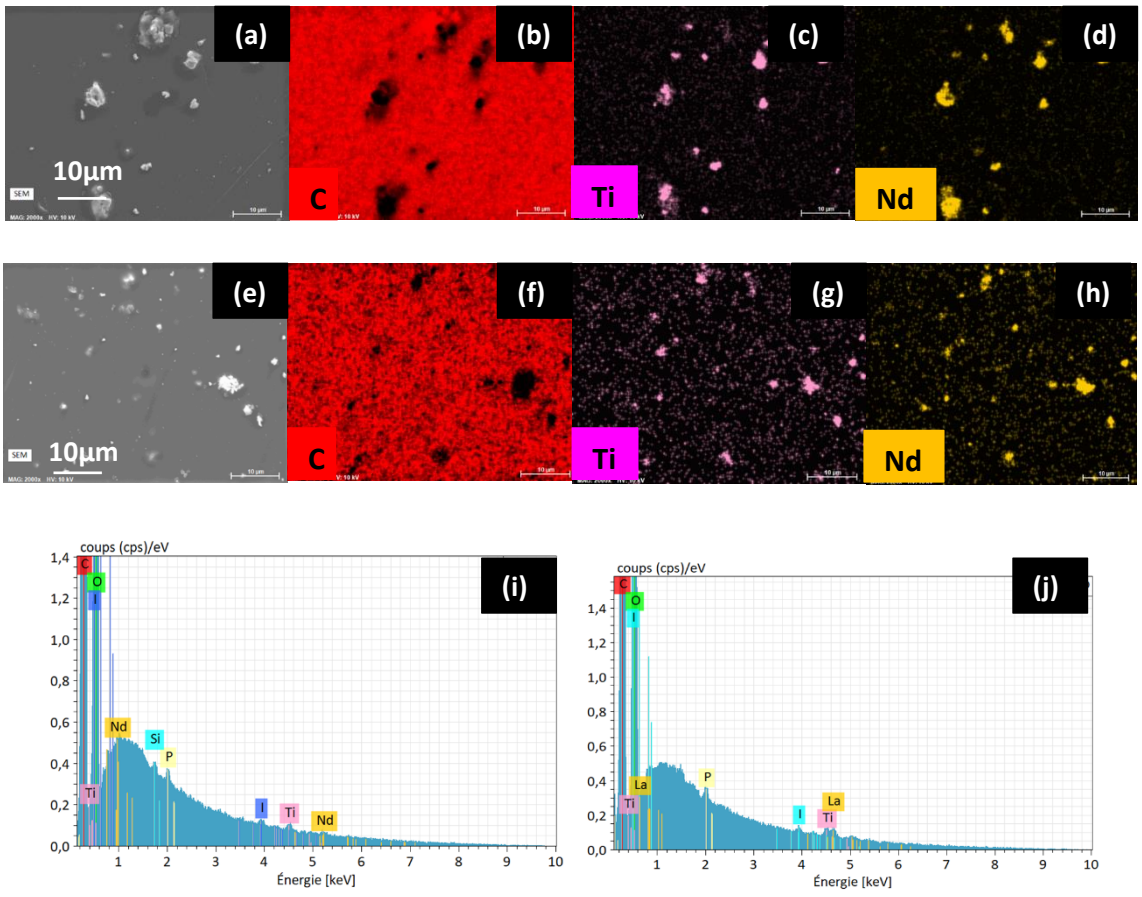

Figure 4. SEM-EDX analysis of (a, b, c, d, i) 2% $Nd_{0.9}TiO_3$/polymer composite, (e, f, g, h, j) 2% $LaTiO_3$/polymer composite.

Figure 4 (a, b, c and e, f, g) presenting the different images resulting from the coupling between the SEM and EDX analyses, verifies the immobilization of the two different perovskites at the neat polymer surface. The obtained cartography describes well the distribution of Nd, La and Ti belonging to the perovskites as well as the carbon of the TMPTA monomer forming the polymer. EDX spectra show also the presence of iodine and phosphorus coming from the photoinitiator system used to initiate the photopolymerization process.

Hence, TEM, SEM and EDX analyses revealed clearly that the perovskites are well incorporated into the polymer matrix by photopolymerization which is a mild polymerization process.

3.3.2. Structural characterization

To be photocatalytically active under light irradiation, the perovskite structures should be preserved even after their encapsulations into the polymer matrix. Therefore, structural stability of these photocatalysts was quantitatively investigated after their immobilizations into the polymers via X-Ray diffraction analysis.

3.3.2.2. X-Ray Diffraction (XRD)

Molecular structures of the as-synthesized composites were studied by realizing XRD analyses. Obtained results are gathered in Figure 5.

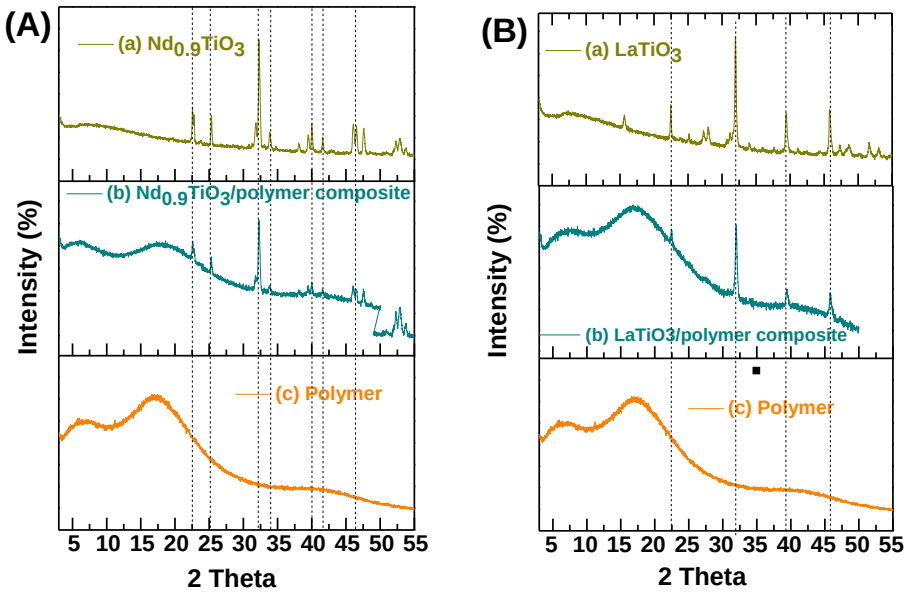

Figure 5. XRD analysis of (A) (a) $Nd_{0.9}TiO_3$, (b) 2% $Nd_{0.9}TiO_3$ /polymer composite, (c) Polymer and (B) (a) $LaTiO_3$, (b) 2% $LaTiO_3$/polymer composite, (c) Polymer.

Figure 5 proves the structural stability of the perovskites after their immobilization into the TMPTA-based polymers. In fact, the most intense peaks present in the perovskite's crystal patterns, characterizing their orthorhombic structures and already reported in the literature[39–41], are also present in the XRD spectra of their respective composites which indicate that no crystallinity changes during the photopolymerization process occur. Moreover, the observed decrease of the perovskite peaks intensities after their incorporations into the polymer matrices is probably due to their low mass percentages equal to (2% w/w).

3.3.3. Surface properties and porosity

3.3.3.1. BET analysis

In order to further understand the photocatalytic process induced by the developed perovskites/polymer composites which occurs at these materials surfaces, it was primordial to investigate the BET surfaces area, the adsorption average pore width and the total area in pores of these photocatalysts. Results are gathered in Table 3.

Table 3. BET surface area and adsorption average pore width of the different perovskites/polymer based TMPTA composites and of the neat polymer.

	BET surface area ($m^2.g^{-1}$)
TMPTA polymer	9.3
0.5% $Nd_{0.9}TiO_3$/polymer	3.8 ± 0.3
1% $Nd_{0.9}TiO_3$/polymer	1.9 ± 0.1
2% $Nd_{0.9}TiO_3$/polymer	1.7± 0.11
0.5% $LaTiO_3$/polymer	1.8 ± 0.1
1% $LaTiO_3$/polymer	1.6 ± 0.1
2% $LaTiO_3$/polymer	5.3 ± 0.7

Immobilization of the perovskites into the TMPTA-based polymer matrices provoked a decrease in its BET surface initially, equal to 9.3 $m^2.g^{-1}$. In fact, polymer BET surface area decreases to 3.8, 1.9 and 1.7 $m^2.g^{-1}$ and to 1.8, 1.6 and 5.3 $m^2.g^{-1}$ by adding 0.5%, 1% and 2% of perovskites $Nd_{0.9}TiO_3$ and $LaTiO_3$, respectively. This could be due to the blocking of the polymer pores by the photocatalysts. Moreover, the chosen perovskites used as photocatalysts are initially non-porous. Further studies will be realized in our group in order to improve BET surface area of these developed materials.

3.3.3.2. Surface topography by AFM

Heterogenous photocatalytic reactions take place at the photocatalysts surface. Therefore, investigation of the roughness and the topography of the different composites via Atomic Force Microscopy was essential to further understand the obtained catalytic performances. Obtained topographical images are presented in Figure 6.

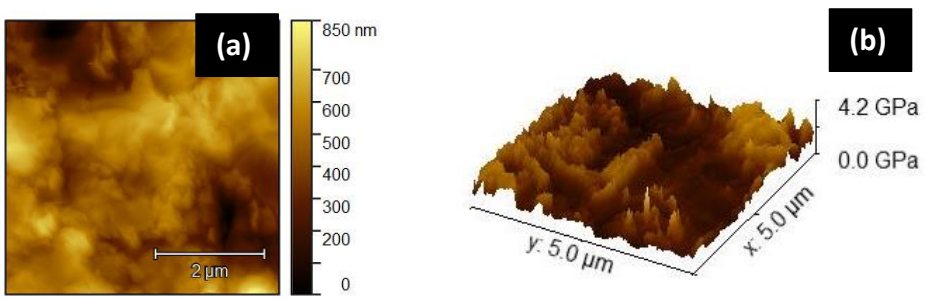

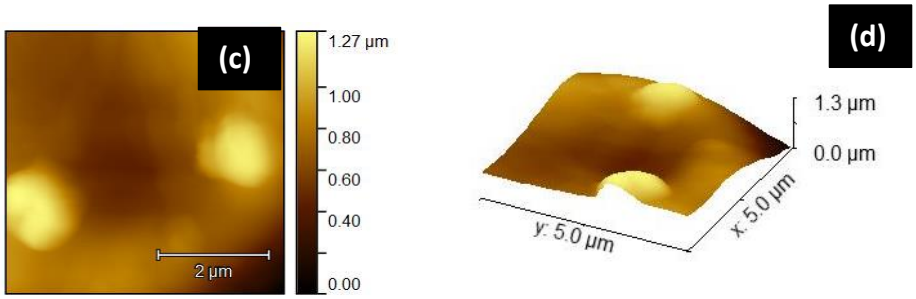

Figure 6. 2D and 3D AFM topology images of (a, b) the 2% $Nd_{0.9}TiO_3$/polymer composite and (c, d) the 2% $LaTiO_3$/polymer composite.

The AFM topographical images of the neat TMPTA-based polymer were already reported in our previous works[50].

In line with the SEM images, Figure 6 corresponding to composites AFM images recorded over an area of 5 µm×5 µm clearly evidence that the polymer surface is affected by the presence of the perovskites playing the role of fillers. Indeed, the roughness average value of this matrix was increased from 5 nm to 153 nm and 109 nm, respectively in the case of the 2% $Nd_{0.9}TiO_3$/polymer and 2% $LaTiO_3$/polymer composites.

One of the main objectives of shaping the chosen perovskites into pellets by their incorporation into polymer matrices, is to facilitate their collect and reuse at the end of the photocatalytic process. Therefore, for practical environment use, the photocatalysts should be characterized by a good mechanical resistance. This parameter was verified by AFM and DMA analysis.

3.3.3.3. Mechanical properties

Mechanical stiffness of the two different synthesized perovskites/polymer composites was examined via Peak-Force QNM imaging mode. Figure 7 displays the elastic modulus on the surface of the synthesized materials recorded over an area of 5 µm×5 µm. The elastic modulus maps of the pure TMPTA-based polymer was already reported in our previous works[50].

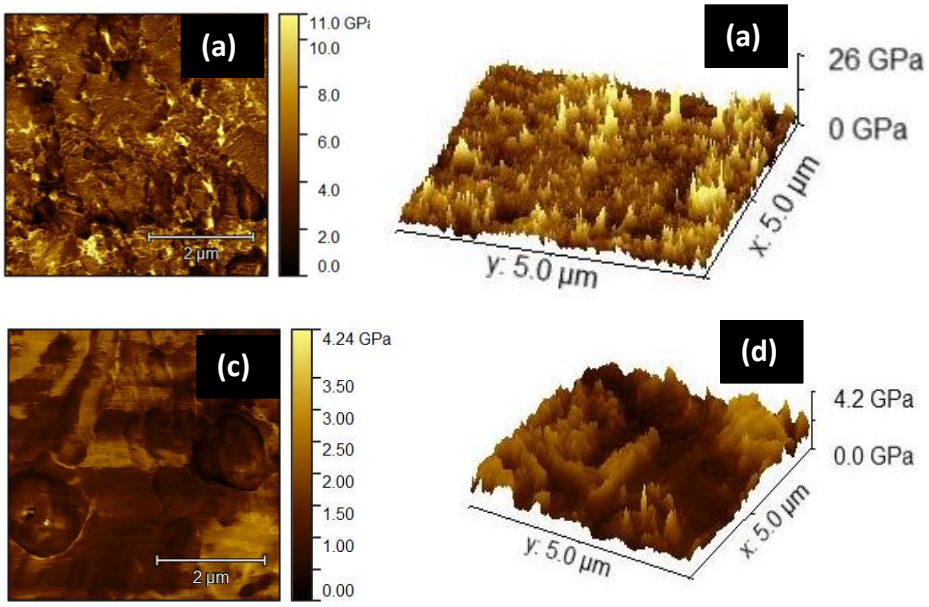

Figure 7. 2D and 3D elastic modulus maps of (a, b) the 2% $Nd_{0.9}TiO_3$/polymer composite and (c, d) the 2% $LaTiO_3$/polymer composite.

The composite rigidity was evaluated by the elastic resistance to AFM indentation. As shown in Figure 7 and based in our previous works, we can assume that the stiffness of the neat polymer is modified by the presence of the perovskites at the surface. Indeed, the mean value of the elastic modulus of the polymer network was slightly decreased from 1.4 GPa to 1.3 GPa in the case of the 2% $LaTiO_3$/polymer composite. However, its rigidity was enhanced to 4.5 in the case of the 2% $Nd_{0.9}TiO_3$/polymer composite. This different alteration of polymers rigidity caused by the perovskite's crystals presence into the polymer network is certainly due to the higher bulk modulus of the $Nd_{0.9}TiO_3$ compared to that of the $LaTiO_3$ perovskite[42].

Since AFM technique estimates only the elastic resistance at the surface of the composites, it was interesting to evaluate the bulk mechanical properties of the developed photocatalysts via Dynamic Mechanical Analysis (DMA). The obtained results are summarized in Table 4.

Table 4. Dynamic storage modulus (G'), dynamic loss modulus (G'') at 25°C of the neat TMPTA based polymer, 2% $Nd_{0.9}TiO_3$/polymer and 2% $LaTiO_3$/polymer composites.

Composition	Dynamic storage modulus G'(MPa)	Dynamic loss modulus G'' (MPa)
Polymer	100	20

2% $Nd_{0.9}TiO_3$/polymer	152	12
2% $LaTiO_3$/polymer	154	10

The values represented in Table 4 elucidate the rigid characters of the neat polymer and the perovskites/polymer composites, since the dynamic storage modulus G' were greater than the dynamic loss modulus G''. This was in line with the high polymerization rates and the low swelling percentages obtained in the case of these materials (See Table 1). Furthermore, an increase of the neat polymer G' was noticed when incorporating the perovskites into this matrix (100MPa vs. 152MPa and 154MPa). The bulk mechanical properties of this material were therefore improved thanks to the high bulk modulus of the perovskites photocatalysts[42]. However, the dynamic loss modulus was decreased from 20MPa to 12MPa and 10MPa in the case of the 2% $Nd_{0.9}TiO_3$/polymer and 2% $LaTiO_3$/polymer composites, respectively which indicates an amelioration of the polymer elastic comportment.

Absorbance domain of the photocatalysts is also one of the most important indexes to consider for the photocatalytic environmental application of such materials. Therefore, it was imperative to investigate the gap energy of the different synthesized materials in order to be able to choose the most appropriate source of irradiation allowing the achievement of relevant photocatalytic results.

3.3.4. Optical properties

UV-visible diffuse reflectance spectra as well as the bandgap energies of the different synthesized materials are shown respectively in Figure 8, Figure S2 and the different date are gathered in Table 5.

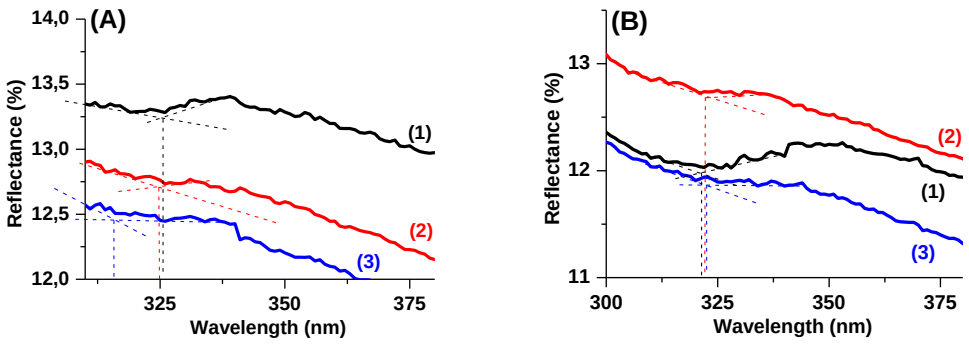

Figure 8. UV-visible diffuse reflectance spectra of (A) (1) 0.5%, (2) 1%, (3) 2% $Nd_{0.9}TiO_3$/polymer composites and (B) (1) 0.5%, (2) 1% and (3) (1) 0.5%, (2) 1%, (3) 2% $LaTiO_3$/polymer composites.

Table 5. Bandgap energy values and maximum absorption wavelengths of the different perovskites/polymer composites and the neat polymer based TMPTA.

	Band Gap energy (eV)	**$\lambda_{(max)}$ (nm)**
Neat Polymer	-	-
1% TiO_2/polymer	3.1	396
0.5% $Nd_{0.9}TiO_3$/polymer	3.8	325
1% $Nd_{0.9}TiO_3$/polymer	3.8	324
2% $Nd_{0.9}TiO_3$/polymer	3.9	315
0.5% $LaTiO_3$/polymer	3.8	321
1% $LaTiO_3$/polymer	3.8	321
2% $LaTiO_3$/polymer	3.8	322

The developed perovskites/polymer composites exhibited high energy bandgap ranging between 3.8 eV and 3.9 eV. The energy bandgap value obtained in the case of the $LaTiO_3$ composite is in line with that already reported for the $LaTiO_3$ crystal which was equal to 3.46 eV[33]. Remarkably, the energy bandgaps of the synthesized photocatalysts weren't affected by the variation of the perovskites mass percentages into the neat polymer (See Table 4). Moreover, since the photocatalytic performances of these materials depend essentially on their absorbance energy, therefore, these perovskites/polymer composites are expected to be more high-performing under UV irradiation devices. Furthermore, the TiO_2/polymer composite exhibits lower energy bandgap (3.1 eV) than the perovskites ones, consequently this photocatalyst should be more efficient under visible light irradiation. Effectiveness of these different synthesized composites for the photocatalytic degradation of a pollutant model i.e. Acid Black will be investigated below.

3.4. Photocatalytic activity of the perovskites/polymer composites

Acid Black dye was chosen as the target pollutant to degrade in order to test the photocatalytic performances of the manufactured perovskites/polymer composites under UV

lamp irradiation since the maximum absorbance wavelengths of these materials corresponds principally to the UV absorbance domain. First of all, the different $LaTiO_3$/polymer composites synthesized using TMPTA, SR-610, PETIA and Ebecryl 40 as the monomers were tested in order to identify the most adequate matrix to use for the incorporation of the perovskites photocatalysts. Results are shown in Figure 9. All degradation experiments were preceded by adsorption tests carried out by keeping the photocatalyst in contact with the Acid Black aqueous solution in the dark during 1 hour. Almost no adsorption of this dye by the developed composites was observed.

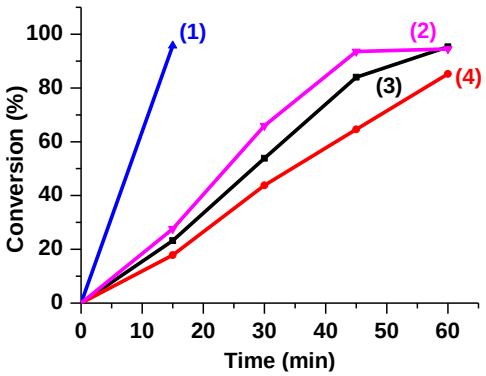

Figure 9. Degradation plot of Acid Black (15 ppm) under UV lamp irradiation (C) in the presence of the 0.5% $LaTiO_3$/polymer composites based on 1) SR-610, (2) TMPTA, (3) PETIA, (4) Ebecryl 40 monomers.

Figure 9 in agreement with Table 1 demonstrates that the most suitable monomer for the development of perovskites/polymer composites with specific application in the photocatalytic field, is TMPTA, since the perovskites composite based on this monomer ensures at the same time, higher Acid Black dye degradation rate and kinetic characterized by a k_{app}=0.035min^{-1} vs. 0.025min^{-1} and 0.019 min^{-1}, respectively in the cases of the PETIA and Ebecryl 40 monomers. Moreover, the fabricated materials based on TMPTA exhibited lower swelling percentages proving a better encapsulation ability of the photocatalysts and therefore a lower risk of their leaching in the environment. The better catalytic performance of the composite based on TMPTA could be explained by the fact that this monomer has a lower viscosity equivalent to 115 mPa/s compared to that of PETIA and Ebecryl 40 equal respectively to 1044 mPa/s and 160 mPa/s. Moreover, compared to TMPTA which has only 3

reactive polymerizable groups, Ebecryl 40 has 4 functionalities, which probably make the perovskites sites less accessible to activate during the dye photodegradation process.

However, concerning the composite synthesized based on the SR-610 monomer, a complete decomposition of the target pollutant obtained in just 15min of UV lamp irradiation is surely due to the important swelling percentage obtained equal to 54% (See Table 1) provoking the leaching of the perovskites into the dye aqueous solution which accelerates the degradation process. This could be explained by its hydrophilic character compared to the others monomers.

In conclusion, we can assume that the best monomer to use for the development of the perovskites/polymer composite is TMPTA, thanks to its hydrophobicity, its medium viscosity and reactive functionalities. The following experiments consisting in studying the effect of the variation of the mass percentages of the perovskites into the polymer, as well as the identification of the mechanism of degradation will be conducted using the composites prepared with TMPTA as the monomer. Obtained results concerning the effect of the perovskites amount encapsulated into the monomer matrix on the degradation percentages of Acid Black are shown in Figure 10.

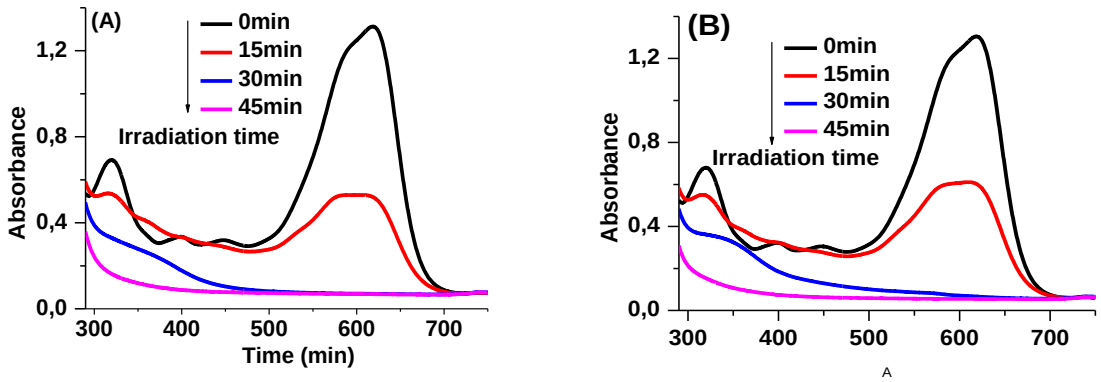

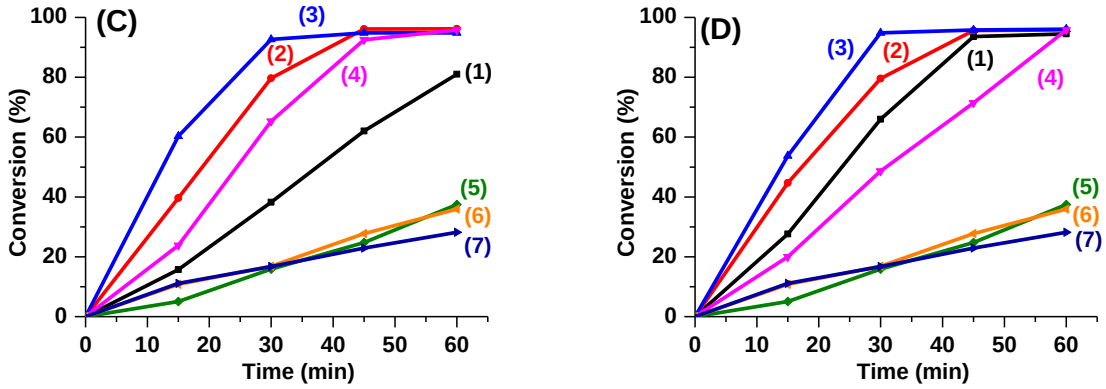

Figure 10. UV-visible absorption spectra of Acid Black water solutions during the photocatalytic degradation process under UV lamp irradiation in the presence of (A) 2% $Nd_{0.9}TiO_3$/polymer composite and (B) 2% $LaTiO_3$/polymer composite. $[AB]_0$ = 15 ppm, pH = 7. Degradation plot of Acid Black (15 ppm) under UV lamp irradiation (C) in the presence of (1) 0.5%, (2) 1%, (3) 2% $Nd_{0.9}TiO_3$/polymer composite, (4) 1% $Nd_{0.9}TiO_3$/polymer composite without iodonium salt, (5) 1%TiO_2/polymer composite, (6) neat polymer, (7) photolysis plot of Acid black without composites and (D) in the presence of (1) 0.5%, (2) 1%, (3) 2% $LaTiO_3$/polymer composites, (4) 1% $LaTiO_3$/polymer without iodonium salt, (5) 1% TiO_2/polymer composite, (6) neat polymer and (7) photolysis plot of Acid black without composites.

Figure 10 (A and B) shows the effect of the perovskites/polymer composites on the absorption spectra of the Acid Black dye which is characterized by two absorbance peaks located at 320 nm and 618 nm reflecting respectively the benzene and naphthalene transitions and the azo group (N = N) transition[43,44]. The second absorbance band is used to monitor the discoloration of the Acid Black dye. Indeed, in the presence of two perovskites/polymer composite and under UV lamp irradiation, a rapid decrease of the absorbance intensity at 618 nm and 320 nm was noticed, stipulating the total degradation of this Acid Black pollutant. Details on the formed intermediates during the photocatalytic treatment were previously reported in our group when degrading Acid Black with MOFs/polymer composites (ref).

In order to compare the effectiveness of the different developed composites on the decomposition of the Acid Black dye, a quantitative kinetics study was carried out by fitting

the pseudo first-order equation to the experimental data. This model is given by the following equation[45]:

$$-Ln(C/C_0) = k_{app}\, t \qquad (1)$$

C and C_0 designate respectively the Acid Black initial concentration and at time t, k_{app} is the first-order rate constant (min^{-1}) and gives an indication of the activity of the catalyst. Results are gathered in Table S1.

Remarkably, after 60 min of UV lamp irradiation photolysis, Acid Black is just decomposed at 26 % (k_{app}=0.005 min^{-1}) and at 35% (k_{app}=0.007 min^{-1}) in the presence of the polymer.

However, the addition of 2% $Nd_{0.9}TiO_3$/polymer and 2% $LaTiO_3$/polymer composite in the Acid Black aqueous solution, enhanced the photodegradation of this dye reaching respectively 94% and 95% vs. 15% in the presence of the neat polymer proving then the high photocatalytic ability of the developed materials. Moreover, by increasing the crystalline $Nd_{0.9}TiO_3$ mass percentages into the polymer from 0.5% to 1% and 2% greatly improved the composite photocatalytic performance. Hence, the degradation percentages were increased from 38% (k_{app}=0.016 min^{-1}) to 94% (k_{app}=0.087 min^{-1}) after 30 min of irradiation (See Figure 10 C (curves 1, 2, 3) and Table S1). Likewise, composites holding 0.5% to 1% and 2% of crystalline $LaTiO_3$ decomposed 65% (k_{app}=0.036 min^{-1}), 79% (k_{app}=0.053 min^{-1}) and 95% (k_{app}=0.099 min^{-1}), respectively under the same irradiation time (See Figure 10 D (curves 1, 2, 3)).

Furthermore, the developed composites exhibited higher catalytic performance compared to the usually used one the TiO_2/polymer composite since only 15% (k_{app}=0.007 min^{-1}) of the Acid Black dye was removed from water after 30 min of UV lamp irradiation. The titanium dioxide composite was synthesized under the same experimental conditions than the perovskites/polymer composites.

5. Proposed photocatalytic degradation mechanism

In order to identify the degradation mechanism of the Acid Black in the presence of the perovskites/polymer composites under UV lamp irradiation, the decomposition kinetics of this dye was monitored in the presence of different scavengers and under different

atmospheres (Air and N_2). For this purpose, EDTA[16,46], isopropanol[47], MEHQ[48] and TEMPO[49] were used in this study respectively as H^+, Hydroxyl radicals ($^{\bullet}OH$), oxygen active species ($RO^{\bullet}$ and $ROO^{\bullet}$) and carbon centered radicals scavengers. Their molar concentrations were fixed to 1 Mm for all the experiments below (See Figure 11).

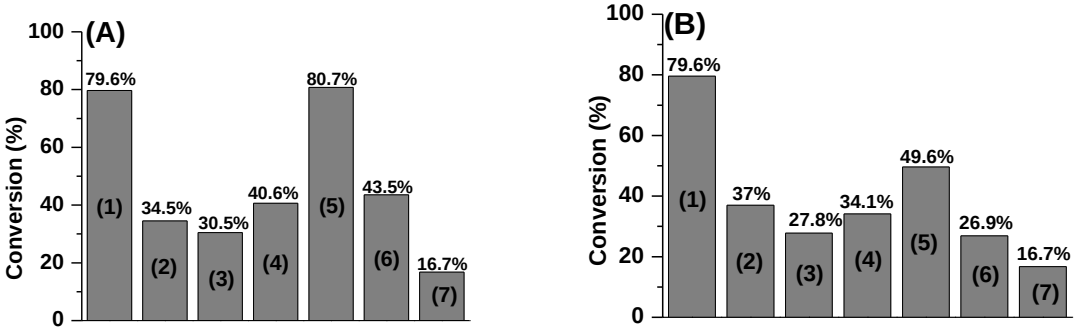

Figure 11. Effects of different scavengers on the degradation of Acid Black under UV lamp irradiation at t = 30 min, in the presence of (A) 1% $Nd_{0.9}TiO_3$/polymer composite and (B) 1% $LaTiO_3$/polymer composite: (1) Without scavengers, under air, (2) Without scavengers, under N_2. Under air, with the addition of (3) TEMPOL, (4) MEHQ, (5) Isopropyl alcohol and (6) EDTA. (7) Without composite, without scavengers.

First of all, the effect of the dissolved oxygen on the kinetics of the Acid Black degradation was investigated. Figure 11 (batons 1 and 2) shows clearly the importance of O_2 on the enhancement of this dye decomposition. Indeed, under N_2 and after 30 min of UV lamp irradiation, the conversion percentages were decreased from 79.6% to 34.5% and 37% in the presence of 1% $Nd_{0.9}TiO_3$/polymer and 1% $LaTiO_3$/polymer composites, respectively. This indicates probably an important role played by $^{\bullet}O_2^-$, formed as a result of the reaction between the excited e^- and the dioxygen dissolved in the solution, during the photocatalytic process.

As for the other oxygenated radical ($RO^{\bullet}$ and $ROO^{\bullet}$), their improvement of the Acid Black photocatalytic process was proved by the decline of the dye conversion percentages from 79.6% to 40.6% and 34.1% respectively is the presence of 1% $Nd_{0.9}TiO_3$/polymer and 1% $LaTiO_3$/polymer composites (See Figure 11 (batons 1 and 4)). However, the hydroxyl radicals seem to be involved in the degradation mechanism of the targeted pollutant in the presence

of the 1% $LaTiO_3$/polymer composite and not in the presence of the second composite (See Figure 11 (batons 1 and 5)).

Furthermore, the holes and carbonated radicals participated also to the Acid Black degradation mechanism. This was pointing out by the decrease of the dye degradation rate when adding EDTA and TEMPOL. In fact, removal rates achieved under 30 min of UV lamp irradiation, equal to 79.6% were diminished respectively to 43.6%, 28.9%, 30.6% and 27.8% respectively in the presence of these two trappers and in the presence of the Neodymium and lanthanum composites (See Figure 11 (batons 1, 3 and 6)).

Similar to the typical semiconductors' behaviors, electrons located in the valence band of a photocatalyst irradiated by an energy equal or higher to its energy bandgap, are excited and transferred to the conduction band forming then electrons-holes pairs which react at their turns with dissolved dioxygen and H_2O molecules present in the aqueous solution to form reactive radicals able to degrade the targeted pollutant. Indeed, $^{\bullet}O_2^-$ which is one of the most reported active species, involved in the photocatalytic processes, could be formed only if the valence band of the photocatalyst is more positive than the oxidation potential of H_2O (1.23 V vs. NHE). $^{\bullet}OH$ is also usually identified as active radicals involved in the organic pollutants degradation pathway[5].

6. Perovskites/polymer composites reusability and stability study

One of the most important objectives of incorporating perovskites into a polymer is the formation of materials easy to collect at the end of the photocatalytic process, to regenerate and to reuse, which makes them more interesting and attractive for environmental practical application. In order to verify the successful achievement of this goal, the shaped perovskites/polymer composites were collected from the spectroscopy UV-visible cuvette containing the Acid Black aqueous solution, they were washed with water, dried in air and then reused for 10 successive photocatalytic degradation cycles. Obtained results are presented in Figure 12.

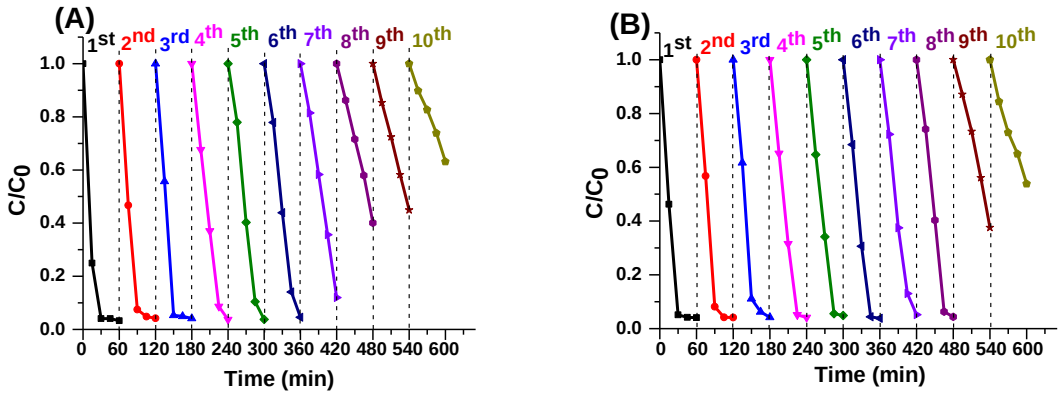

Figure 12. Ten consecutive Acid Black photodegradation cycles over (A) 2% $Nd_{0.9}TiO_3$/polymer composite and (B) 2% $LaTiO_3$/polymer composite. $[AB]_0$=15ppm, pH=7, irradiation source: UV Lamp.

Figure 12 highlights the fruitful association between the perovskites and the TMPTA-based polymer, which allowed the obtention of shaped materials with enhanced mechanical properties easy and cheap to recover and to reuse without external regeneration, avoiding then the usual time-consuming regeneration methods. Indeed, the developed materials kept their high photocatalytic efficiency for several successive catalytic cycles which starts to decrease from the 8th and 9th cycles respectively in the case of the 2%$Nd_{0.9}TiO_3$/polymer and 2%$LaTiO_3$/polymer composites (See Figure 12 (A and B)).

Furthermore, photostability of the synthesized photocomposites based on perovskites were examined by comparing SEM and XRD characterizations images and spectra before and after the photocatalytic processes (See Figures 13 and 14).

Figure 13 (a, b) proves the photostability of the developed photocatalysts. In fact, the photocomposites surface remains intact after 60 min of UV lamp irradiation (See Figure 13). The SEM-EDX images of the different developed photocomposites taken after one photocatalytic cycle and shown in Figure S1 (e, f, g, h, i, j) as well as the cutaway views, verify also the presence of the perovskites at the surface and in the bulk of the polymer matrix.

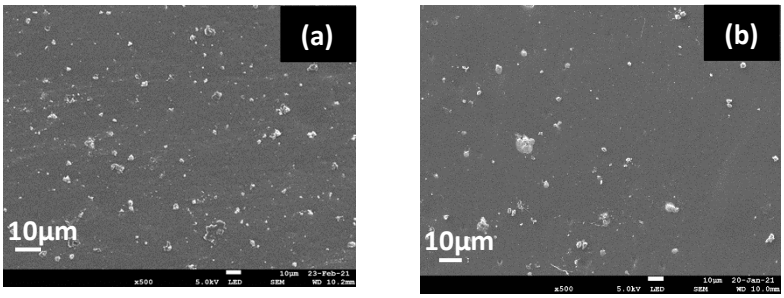

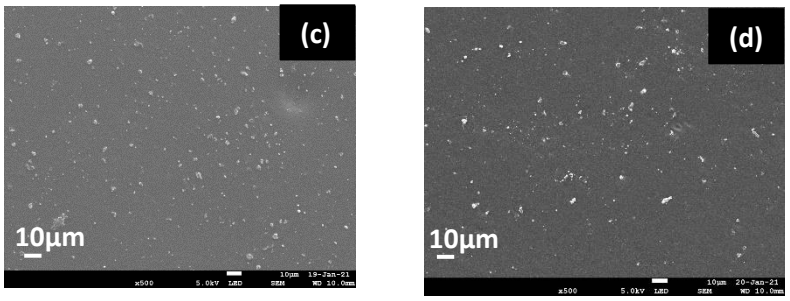

Figure 13. SEM-EDX images of 2% $Nd_{0.9}TiO_3$/polymer composite (a) before and (b) after one photodegradation cycle. SEM-EDX images of 2% $LaTiO_3$/polymer composite (c) before and (d) after one photodegradation cycle.

Conclusions

In conclusion, this study reports the successful hybridization between perovskites and polymer via a facile, low-cost, rapid and ecofriendly photopolymerization process under mild visible Light Emitting Diode LED@405nm. This fruitful association allowed the obtention of

shaped materials easy to collect and to recycle without external usual and time-consuming regeneration methods. Indeed, the two perovskites/polymer composites were effective for the photodegradation of the Acid Black dye for several successive cycles.

Four different monomers were tested during the synthesis of the composites. TMPTA, was the most suitable one thanks to its medium viscosity and to its three available reactive functionalities allowing the achievement of high polymerization percentages. Moreover, the composites based on TMPTA monomer were stable in water.

The fabricated immobilized perovskites exhibited higher photocatalytic activity under UV lamp irradiation than the universal used photocatalyst the TiO_2. In fact, approximatively 94% and 95% of the target chosen dye was removed from water after just 30 min of irradiation in the presence of respectively 2% $Nd_{0.9}TiO_3$/polymer and 2% $LaTiO_3$/polymer composites, compared to 15% degraded by the 1% TiO_2/polymer composite synthesized under the same experimental conditions than the other composites. Also, to further understand the degradation mechanism of the chosen pollutant, kinetics degradation was monitored in the presence of various radical scavengers and under different atmospheres. The results demonstrated that the degradation percentages were decreased under N_2 atmosphere proving the important role played by the dissolved oxygen on the enhancement of the catalytic degradation of the Acid Black dye.

The new as-synthesized materials were fully characterized by numerous techniques including SEM, TEM, EDX, DRX which have proved the successful hybridization of perovskites/polymer composites. Furthermore, the shaped obtained materials exhibited high rigidity and high thermal stability, investigated respectively by AFM, DMA and ATG methods.

In conclusion, this work proved once again the facility and the pertinence of our new developed methodology for the synthesis and the characterization of various photocatalysts/polymer composites by obtaining molded materials assembling at the same time the high processability of the polymer and the excellent photocatalytic activity of the photocatalysts. Associating perovskites with polymer by a simple photopolymerization process could promotes their environmental practical application and therefore their commercialization.

Table of contents Graphic (TOC)

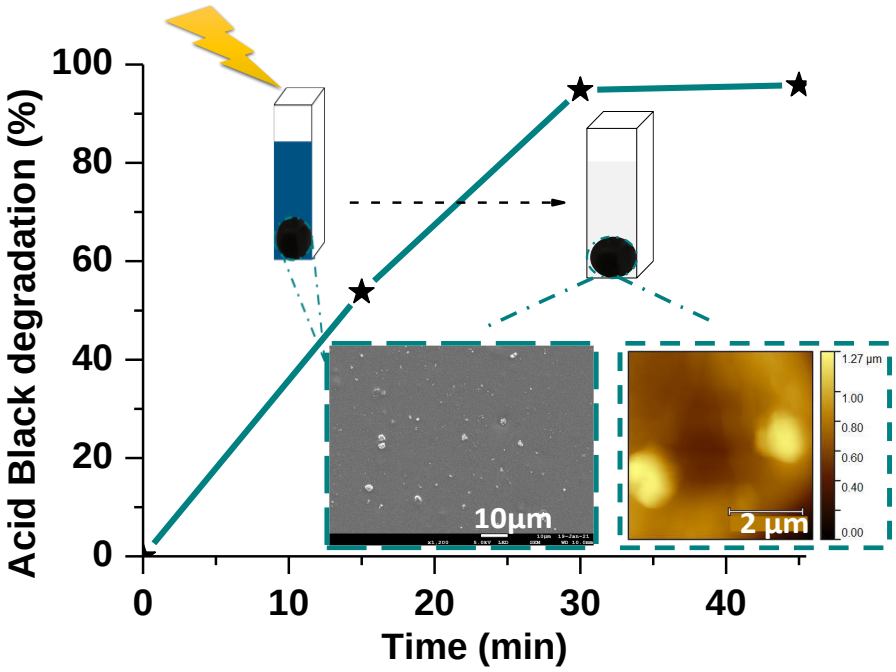
Acid Black degradation (%)
100
80
60
40
20
0
0
10
20
30
40
Time (min)
10µm
2 µm
1.27 µm
1.00
0.80
0.60
0.40
0.00

References

(1) Yahya, N.; Aziz, F.; Jamaludin, N. A.; A. Mutalib, M.; Ismail, A. F.; W. Salleh, W. N.; Jaafar, J.; Yusof, N.; A. Ludin, N. A Review of Integrated Photocatalyst Adsorbents for Wastewater Treatment. *Journal of Environmental Chemical Engineering* **2018**, *6* (6), 7411–7425. https://doi.org/10.1016/j.jece.2018.06.051.

(2) Zhang, J.; Hu, W.; Cao, S.; Piao, L. Recent Progress for Hydrogen Production by Photocatalytic Natural or Simulated Seawater Splitting. *Nano Res.* **2020**, *13* (9), 2313–2322. https://doi.org/10.1007/s12274-020-2880-z.

(3) Gao, Y.; Qian, K.; Xu, B.; Li, Z.; Zheng, J.; Zhao, S.; Ding, F.; Sun, Y.; Xu, Z. Recent Advances in Visible-Light-Driven Conversion of CO2 by Photocatalysts into Fuels or Value-Added Chemicals. *Carbon Resources Conversion* **2020**, *3*, 46–59. https://doi.org/10.1016/j.crcon.2020.02.003.

(4) Ângelo, J.; Andrade, L.; Madeira, L. M.; Mendes, A. An Overview of Photocatalysis Phenomena Applied to NOx Abatement. *Journal of Environmental Management* **2013**, *129*, 522–539. https://doi.org/10.1016/j.jenvman.2013.08.006.

(5) Bresolin, B.-M.; Ben Hammouda, S.; Sillanpää, M. An Emerging Visible-Light Organic–Inorganic Hybrid Perovskite for Photocatalytic Applications. *Nanomaterials* **2020**, *10* (1), 115. https://doi.org/10.3390/nano10010115.

(6) Li, F.; Kang, Y.; Chen, M.; Liu, G.; Lv, W.; Yao, K.; Chen, P.; Huang, H. Photocatalytic Degradation and Removal Mechanism of Ibuprofen via Monoclinic BiVO4 under Simulated Solar Light. *Chemosphere* **2016**, *150*, 139–144. https://doi.org/10.1016/j.chemosphere.2016.02.045.

(7) Zhang, X.; Wang, Y.; Hou, F.; Li, H.; Yang, Y.; Zhang, X.; Yang, Y.; Wang, Y. Effects of Ag Loading on Structural and Photocatalytic Properties of Flower-like ZnO Microspheres. *Applied Surface Science* **2017**, *391*, 476–483. https://doi.org/10.1016/j.apsusc.2016.06.109.

(8) Tong, T.; Zhang, J.; Tian, B.; Chen, F.; He, D. Preparation of Fe3+-Doped TiO2 Catalysts by Controlled Hydrolysis of Titanium Alkoxide and Study on Their Photocatalytic Activity for Methyl Orange Degradation. *Journal of Hazardous Materials* **2008**, *155* (3), 572–579. https://doi.org/10.1016/j.jhazmat.2007.11.106.

(9) Shivaraju, H. P.; Midhun, G.; Anil Kumar, K. M.; Pallavi, S.; Pallavi, N.; Behzad, S. Degradation of Selected Industrial Dyes Using Mg-Doped TiO2 Polyscales under Natural

Sun Light as an Alternative Driving Energy. *Appl Water Sci* **2017**, *7* (7), 3937–3948. https://doi.org/10.1007/s13201-017-0546-0.

(10) Nam, Y.; Lim, J. H.; Ko, K. C.; Lee, J. Y. Photocatalytic Activity of TiO_2 Nanoparticles: A Theoretical Aspect. *J. Mater. Chem. A* **2019**, *7* (23), 13833–13859. https://doi.org/10.1039/C9TA03385H.

(11) Dodd, A.; McKinley, A.; Tsuzuki, T.; Saunders, M. Optical and Photocatalytic Properties of Nanoparticulate (TiO2)x(ZnO)1−x Powders. *Journal of Alloys and Compounds* **2010**, *489* (2), L17–L21. https://doi.org/10.1016/j.jallcom.2009.09.126.

(12) Xu, J.; Ao, Y.; Fu, D.; Yuan, C. Synthesis of Gd-Doped TiO2 Nanoparticles under Mild Condition and Their Photocatalytic Activity. *Colloids and Surfaces A: Physicochemical and Engineering Aspects* **2009**, *334* (1–3), 107–111. https://doi.org/10.1016/j.colsurfa.2008.10.017.

(13) Sakthivel, S.; Kisch, H. Daylight Photocatalysis by Carbon-Modified Titanium Dioxide. *Angew. Chem. Int. Ed.* **2003**, *42* (40), 4908–4911. https://doi.org/10.1002/anie.200351577.

(14) Chen, X.; Wu, Z.; Liu, D.; Gao, Z. Preparation of ZnO Photocatalyst for the Efficient and Rapid Photocatalytic Degradation of Azo Dyes. *Nanoscale Research Letters* **2017**, *12* (1), 143. https://doi.org/10.1186/s11671-017-1904-4.

(15) Luo, J.; Hepel, M. Photoelectrochemical Degradation of Naphthol Blue Black Diazo Dye on WO3 Film Electrode. *Electrochimica Acta* **2001**, *46* (19), 2913–2922. https://doi.org/10.1016/S0013-4686(01)00503-5.

(16) Senasu, T.; Nanan, S. Photocatalytic Performance of CdS Nanomaterials for Photodegradation of Organic Azo Dyes under Artificial Visible Light and Natural Solar Light Irradiation. *J Mater Sci: Mater Electron* **2017**, *28* (23), 17421–17441. https://doi.org/10.1007/s10854-017-7676-x.

(17) Rao, H.; Lu, Z.; Liu, X.; Ge, H.; Zhang, Z.; Zou, P.; He, H.; Wang, Y. Visible Light-Driven Photocatalytic Degradation Performance for Methylene Blue with Different Multi-Morphological Features of ZnS. *RSC Adv.* **2016**, *6* (52), 46299–46307. https://doi.org/10.1039/C6RA05212F.

(18) Ghali, M.; Brahmi, C.; Benltifa, M.; Dumur, F.; Duval, S.; Simonnet-Jégat, C.; Morlet-Savary, F.; Jellali, S.; Bousselmi, L.; Lalevée, J. New Hybrid Polyoxometalate/Polymer

Composites for Photodegradation of Eosin Dye. *Journal of Polymer Science Part A: Polymer Chemistry* **2019**, *57* (14), 1538–1549. https://doi.org/10.1002/pola.29416.

(19) Li, Y.; Xu, H.; Ouyang, S.; Ye, J. Metal–Organic Frameworks for Photocatalysis. *Phys. Chem. Chem. Phys.* **2016**, *18* (11), 7563–7572. https://doi.org/10.1039/C5CP05885F.

(20) Huang, H.; Pradhan, B.; Hofkens, J.; Roeffaers, M. B. J.; Steele, J. A. Solar-Driven Metal Halide Perovskite Photocatalysis: Design, Stability, and Performance. *ACS Energy Lett.* **2020**, *5* (4), 1107–1123. https://doi.org/10.1021/acsenergylett.0c00058.

(21) Das, N.; Kandimalla, S. Application of Perovskites towards Remediation of Environmental Pollutants: An Overview: A Review on Remediation of Environmental Pollutants Using Perovskites. *Int. J. Environ. Sci. Technol.* **2017**, *14* (7), 1559–1572. https://doi.org/10.1007/s13762-016-1233-7.

(22) Eskandari, N.; Nabiyouni, G.; Masoumi, S.; Ghanbari, D. Preparation of a New Magnetic and Photo-Catalyst CoFe2O4–SrTiO3 Perovskite Nanocomposite for Photo-Degradation of Toxic Dyes under Short Time Visible Irradiation. *Composites Part B: Engineering* **2019**, *176*, 107343. https://doi.org/10.1016/j.compositesb.2019.107343.

(23) Dandia, A.; Saini, P.; Sharma, R.; Parewa, V. Visible Light Driven Perovskite-Based Photocatalysts: A New Candidate for Green Organic Synthesis by Photochemical Protocol. *Current Research in Green and Sustainable Chemistry* **2020**, *3*, 100031. https://doi.org/10.1016/j.crgsc.2020.100031.

(24) Zhou, Y.; Chen, J.; Bakr, O. M.; Mohammed, O. F. Metal Halide Perovskites for X-Ray Imaging Scintillators and Detectors. *ACS Energy Lett.* **2021**, *6* (2), 739–768. https://doi.org/10.1021/acsenergylett.0c02430.

(25) Petrović, M.; Chellappan, V.; Ramakrishna, S. Perovskites: Solar Cells & Engineering Applications – Materials and Device Developments. *Solar Energy* **2015**, *122*, 678–699. https://doi.org/10.1016/j.solener.2015.09.041.

(26) Adjokatse, S.; Fang, H.-H.; Loi, M. A. Broadly Tunable Metal Halide Perovskites for Solid-State Light-Emission Applications. *Materials Today* **2017**, *20* (8), 413–424. https://doi.org/10.1016/j.mattod.2017.03.021.

(27) Ismael, M.; Wark, M. Perovskite-Type LaFeO3: Photoelectrochemical Properties and Photocatalytic Degradation of Organic Pollutants Under Visible Light Irradiation. *Catalysts* **2019**, *9* (4), 342. https://doi.org/10.3390/catal9040342.

(28) Ernawati, L.; Wahyuono, R. A.; Widiyandari, H.; Risanti, D. D.; Yusariarta, A. W.; Rebeka; Sitompul, V. Experimental Data of CaTiO3 Photocatalyst for Degradation of Organic Pollutants (Brilliant Green Dye) – Green Synthesis, Characterization and Kinetic Study. *Data in Brief* **2020**, *32*, 106099. https://doi.org/10.1016/j.dib.2020.106099.

(29) Raja, S. N.; Bekenstein, Y.; Koc, M. A.; Fischer, S.; Zhang, D.; Lin, L.; Ritchie, R. O.; Yang, P.; Alivisatos, A. P. Encapsulation of Perovskite Nanocrystals into Macroscale Polymer Matrices: Enhanced Stability and Polarization. *ACS Appl. Mater. Interfaces* **2016**, *8* (51), 35523–35533. https://doi.org/10.1021/acsami.6b09443.

(30) Tehfe, M.; Louradour, F.; Lalevée, J.; Fouassier, J.-P. Photopolymerization Reactions: On the Way to a Green and Sustainable Chemistry. *Applied Sciences* **2013**, *3* (2), 490–514. https://doi.org/10.3390/app3020490.

(31) Teh, Y. W.; Chee, M. K. T.; Kong, X. Y.; Yong, S.-T.; Chai, S.-P. An Insight into Perovskite-Based Photocatalysts for Artificial Photosynthesis. *Sustainable Energy Fuels* **2020**, *4* (3), 973–984. https://doi.org/10.1039/C9SE00526A.

(32) Bradha, M.; Vijayaraghavan, T.; Suriyaraj, S. P.; Selvakumar, R.; Ashok, A. M. Synthesis of Photocatalytic La(1–x)AxTiO3.5–δ (A=Ba, Sr, Ca) Nano Perovskites and Their Application for Photocatalytic Oxidation of Congo Red Dye in Aqueous Solution. *Journal of Rare Earths* **2015**, *33* (2), 160–167. https://doi.org/10.1016/S1002-0721(14)60397-5.

(33) Shawky, A.; Mohamed, R. M.; Mkhalid, I. A.; Youssef, M. A.; Awwad, N. S. Visible Light-Responsive Ag/LaTiO3 Nanowire Photocatalysts for Efficient Elimination of Atrazine Herbicide in Water. *Journal of Molecular Liquids* **2020**, *299*, 112163. https://doi.org/10.1016/j.molliq.2019.112163.

(34) Saroyan, H.; Kyzas, G.; Deliyanni, E. Effective Dye Degradation by Graphene Oxide Supported Manganese Oxide. *Processes* **2019**, *7*, 40. https://doi.org/10.3390/pr7010040.

(35) Rauf, M. A.; Meetani, M. A.; Hisaindee, S. An Overview on the Photocatalytic Degradation of Azo Dyes in the Presence of TiO2 Doped with Selective Transition Metals. *Desalination* **2011**, *276* (1), 13–27. https://doi.org/10.1016/j.desal.2011.03.071.

(36) Ghali, M.; Brahmi, C.; Benltifa, M.; Vaulot, C.; Airoudj, A.; Fioux, P.; Dumur, F.; Simonnet-Jégat, C.; Morlet-Savary, F.; Jellali, S.; Bousselmi, L.; Lalevée, J. Characterization of Polyoxometalate/Polymer Photo-composites: A Toolbox for the Photodegradation of

Organic Pollutants. *Journal of Polymer Science* **2020**, pol.20200568. https://doi.org/10.1002/pol.20200568.

(37) Ghali, M. Conception et Synthèse de Matériaux Nanostructurés : Application Au Traitement Des Polluants Émergents Par Photodégradation. November 2020.

(38) Omidian, H.; Hasherni, S.; Askari, F.; Nafisi, S. *Swelling and Crosslink Density Measurements for Hydrogels*; 1993.

(39) Herrera, G.; Jiménez-Mier, J.; Chavira, E. Layered-Structural Monoclinic–Orthorhombic Perovskite La2Ti2O7 to Orthorhombic LaTiO3 Phase Transition and Their Microstructure Characterization. *Materials Characterization* **2014**, *89*, 13–22. https://doi.org/10.1016/j.matchar.2013.12.013.

(40) Pan, T.-M.; Shu, W.-H. Structural and Electrical Characteristics of a High-k NdTiO3 Gate Dielectric. *Appl. Phys. Lett.* **2007**, *91* (17), 172904. https://doi.org/10.1063/1.2800307.

(41) Chen, Y.; Xu, J.; Cui, Y.; Shang, G.; Qian, J.; Yao, J. Improvements of Dielectric Properties of Cu Doped LaTiO3+δ. *Progress in Natural Science: Materials International* **2016**, *26* (2), 158–162. https://doi.org/10.1016/j.pnsc.2016.03.001.

(42) Materials Project https://materialsproject.org/#search/materials/{%22reduced_cell_formula%22%3A%22LaTiO3%22} (accessed Mar 26, 2021).

(43) Bechiri, O.; Abbessi, M. Catalytic Oxidation of Naphtol Blue Black in Water: Effect of Operating Parameters and the Type of Catalyst. *Journal of Water and Environmental Nanotechnology* **2017**, *2* (1), 9–16. https://doi.org/10.7508/jwent.2017.01.002.

(44) Onder, S.; Celebi, M.; Altikatoglu, M.; Hatipoglu, A.; Kuzu, H. Decolorization of Naphthol Blue Black Using the Horseradish Peroxidase. *Appl Biochem Biotechnol* **2011**, *163* (3), 433–443. https://doi.org/10.1007/s12010-010-9051-8.

(45) Zhang, H.; Liu, D.; Ren, S.; Zhang, H. Kinetic Studies of Direct Blue Photodegradation over Flower-like TiO2. *Res Chem Intermed* **2017**, *43* (3), 1529–1542. https://doi.org/10.1007/s11164-016-2713-6.

(46) Pedrosa, M.; Da Silva, E. S.; Pastrana-Martínez, L. M.; Drazic, G.; Falaras, P.; Faria, J. L.; Figueiredo, J. L.; Silva, A. M. T. Hummers' and Brodie's Graphene Oxides as Photocatalysts for Phenol Degradation. *Journal of Colloid and Interface Science* **2020**, *567*, 243–255. https://doi.org/10.1016/j.jcis.2020.01.093.

(47) Tang, L.; Jia, C.; Xue, Y.; Li, L.; Wang, A.; Xu, G.; Liu, N.; Wu, M. Fabrication of Compressible and Recyclable Macroscopic G-C3N4/GO Aerogel Hybrids for Visible-Light Harvesting: A Promising Strategy for Water Remediation. *Applied Catalysis B: Environmental* **2017**, *219*, 241–248. https://doi.org/10.1016/j.apcatb.2017.07.053.

(48) Cutié, S. S.; Henton, D. E.; Powell, C.; Reim, R. E.; Smith, P. B.; Staples, T. L. The Effects of MEHQ on the Polymerization of Acrylic Acid in the Preparation of Superabsorbent Gels. *Journal of Applied Polymer Science* **1997**, *64* (3), 577–589. https://doi.org/10.1002/(SICI)1097-4628(19970418)64:3<577::AID-APP14>3.0.CO;2-V.

(49) Liang, J.; Liu, F.; Li, M.; Liu, W.; Tong, M. Facile Synthesis of Magnetic Fe3O4@BiOI@AgI for Water Decontamination with Visible Light Irradiation: Different Mechanisms for Different Organic Pollutants Degradation and Bacterial Disinfection. *Water Research* **2018**, *137*, 120–129. https://doi.org/10.1016/j.watres.2018.03.027.